(Received 4 May 2025, Accepted 23 June 2025, Scheduled 5 July 2025)

Integration of Adaptive Cross Approximation and Generalized Orthogonal Matching Pursuit for Monostatic Electromagnetic Scattering Analysis

Chenggang Wu[1], Zhonggen Wang[1,*], Wenyan Nie[2], Dai Dong[1], and Yang Liu[1]

[1] *School of Electrical and Information Engineering, Anhui University of Science and Technology, Huainan 232001, China*
[2] *School of Mechanical and Electrical Engineering, Huainan Normal University, Huainan 232001, China*

ABSTRACT: A novel dual compressive sensing (DCS) method is presented to resolve the limitations in computational accuracy and efficiency encountered by conventional DCS approaches during monostatic electromagnetic scattering analysis. Based on the connection between adaptive cross approximation (ACA) and generalized orthogonal matching pursuit (gOMP) in DCS, the integration of ACA and gOMP into the DCS framework is implemented. Specifically, ACA is employed to construct a deterministic measurement matrix by extracting row indexes containing critical information from the impedance matrix. This method reduces column correlation in the measurement matrix, enabling fewer rows to achieve comparable accuracy. Furthermore, the gOMP algorithm is adopted for signal recovery, leveraging its multi-column selection mechanism to better utilize the optimized information from ACA, thereby enhancing reconstruction accuracy and efficiency. Numerical analysis demonstrates that the proposed method achieves a significant enhancement in both accuracy and efficiency.

1. INTRODUCTION

The method of moments (MoM) is a highly effective numerical method for analyzing electromagnetic scattering problems, as it discretizes integral equations of electromagnetic fields into matrix equation. However, the computational cost becomes prohibitively high when targets are analyzed with a large number of unknowns. To address these challenges, various acceleration algorithms have been developed, including the Multi-Level Fast Multipole Method (MLFMM) [1], characteristic basis function method (CBFM) [2, 3], and synthetic basis function method (SBFM) [4].

In recent years, compressive sensing (CS) [5–8] has been introduced into MoM, resulting in a promising method for analyzing electromagnetic scattering problems known as compressive sensing-method of moments (CS-MoM) [9]. CS-MoM consists of two models when analyzing problems of electromagnetic scattering characteristics. One model deals with monostatic scattering problems [10, 11], and it aims to minimize the number of matrix equations to be solved. The other model addresses bistatic scattering problems [12, 13], in which the matrix equation is transformed into an underdetermined equation, accelerating the solution.

When addressing the second model for solving electromagnetic scattering problems in three-dimensional (3D) conductors, several methods to enhance computational efficiency have emerged. For instance, in constructing sparse basis, the methods proposed for constructing sparse basis are Krylov subspace basis functions [14, 15] and characteristic models (CMs) [16, 17]. In the other core technology, constructing the measurement matrix, the row elements of the impedance matrix are typically extracted randomly [18], uniformly [17], and using the adaptive cross approximation (ACA) row index [19]. As for the first model, researchers reduce the number of equations that need to be solved by randomly combining incident excitations from different angles to form a new incident source [20]. Based on these findings, [21] proposes a dual compressive sensing (DCS) method; however, since the surface integral equations of the 3D targets are usually discretized by Rao-Wilton-Glisson (RWG) basic functions, resulting in induced currents that are not sparse on the general level, the method can only be used to analyze the electromagnetic scattering problems for two-dimensional (2D) targets. Therefore, [22] proposes a novel DCS method to solve the monostatic scattering problem for 3D targets. However, the method still uses randomly extracted rows of the impedance matrix to construct the measurement matrix and uses the orthogonal matching pursuit (OMP) to reconstruct the currents. Therefore, both computational accuracy and efficiency require enhancement. Ref. [23] also proposes a DCS method that incorporates ACA to accelerate the filling of the excitation matrix, thereby reducing memory usage and computational cost.

It is worth noting that the principles of compressed representation and selective sampling extend beyond electromagnetic scattering. In materials modeling, recent efforts have focused on developing structure-aware, efficient algorithms for predictive modeling, often using compressed data and smart sampling strategies. For example, Zhang et al. provide a comprehensive

* Corresponding author: Zhonggen Wang (zgwang@ahu.edu.cn).

overview of machine learning-based interatomic potentials and highlight the importance of well-designed sampling and reconstruction schemes [24]. This broader perspective underscores the relevance of compressed sensing approaches across various fields of computational science.

A novel method based on a DCS framework combined with ACA is proposed in this paper. Ref. [19] primarily utilizes ACA row indices as a prerequisite for the second-layer ACA, without specific optimization for computational accuracy. In contrast, the ACA row index method proposed in this paper emphasizes its integration with the signal recovery algorithm. During each iteration of gOMP, the low column correlation of the ACA-constructed measurement matrix is fully exploited, enabling bidirectional optimization that significantly enhances computational accuracy. Firstly, a measurement matrix is constructed using the row indices generated by the ACA algorithm, replacing the traditional method of randomly selecting rows from the impedance matrix and serving as the basis for extracting the corresponding rows. Subsequently, given the correlation between the measurement matrix constructed by ACA and Generalized Orthogonal Matching Pursuit (gOMP) algorithm, we have replaced the reconstruction algorithm in the second layer of the DCS framework with the gOMP algorithm. The ACA algorithm constructs the measurement matrix by extracting key row indices, generating a deterministic matrix with low column correlation, whose reconstruction coefficients provide efficient excitation for the second layer. Compared to the single-column selection mechanism of OMP, the multi-column selection mechanism of gOMP, when being combined with ACA, can fully leverage the information from the first layer, thereby significantly enhancing both computational efficiency and accuracy. Compared with [23], our method is dedicated to optimizing the entire compressive-sensing pipeline — not only matrix filling, but, more importantly, the measurement-matrix construction and signal-recovery stages within the DCS process. Such end-to-end optimization is more conducive to subsequent research and improvements. By contrast, [23] merely uses ACA to accelerate the filling of the sensing matrix, which indeed reduces time and memory costs but does not systematically optimize the DCS framework. Moreover, because accelerated matrix-filling operations can be applied in many contexts, our method's optimization of the entire DCS framework not only lowers time costs and enhances accuracy but also provides a solid foundation for further integration of these accelerated matrix-filling techniques, enabling additional performance gains. The effectiveness of the proposed method is demonstrated by theoretical analysis and numerical simulations.

2. THEORY

2.1. Dual Compressive Sensing Theory

From the MoM of monostatic scattering analysis, the equation can be derived as shown below [22]:

$$\mathbf{Z}_{N\times N}\left[\mathbf{I}_1\ \mathbf{I}_2\ \cdots\ \mathbf{I}_R\right]_{N\times R}=\left[\mathbf{V}_1\ \mathbf{V}_2\ \cdots\ \mathbf{V}_R\right]_{N\times R} \tag{1}$$

where N represents the number of RWG basis functions, and $\mathbf{Z}$ is the impedance matrix of dimension $N\times N$. Moreover, $\mathbf{V}_1$ to $\mathbf{V}_R$ are the excitations at R discrete incident angles, and $\mathbf{I}_1$ to $\mathbf{I}_R$ are the corresponding induced currents. Furthermore, transposing both sides of the equation and left multiplying the Gaussian matrix $\mathbf{\Phi}$ of size $r\times R$ yields the following output:

$$\mathbf{\Phi}_{r\times R}\begin{bmatrix}\mathbf{I}_1\\ \mathbf{I}_2\\ \vdots\\ \mathbf{I}_R\end{bmatrix}_{R\times N}[\mathbf{Z}^T]_{N\times N}=\mathbf{\Phi}_{r\times R}\begin{bmatrix}\mathbf{V}_1\\ \mathbf{V}_2\\ \vdots\\ \mathbf{V}_R\end{bmatrix}_{R\times N} \tag{2}$$

where r represents the number of randomly selected angles, and the $\mathbf{\Phi}$ refers to a random matrix whose elements are independently and identically distributed according to the standard normal distribution. To achieve current sparsity, a sparse basis implementation is employed. Within this framework, the discrete cosine transform (DCT) matrix $\mathbf{\Phi}$ serves as the designated representation basis for the induced current, which can be mathematically formulated as follows:

$$\begin{bmatrix}\mathbf{I}_1\\ \mathbf{I}_2\\ \vdots\\ \mathbf{I}_R\end{bmatrix}_{R\times N}=\mathbf{\Psi}_{R\times R}\begin{bmatrix}\varepsilon_1\\ \varepsilon_2\\ \vdots\\ \varepsilon_R\end{bmatrix}_{R\times N} \tag{3}$$

where $[\varepsilon_1\cdots\varepsilon_2\cdots\cdots\varepsilon_R]^T_{R\times N}$ represents the vector of coefficients of the induced current over the sparse basis $\mathbf{\Psi}$. And the size of $\mathbf{\Psi}$ is $R\times R$; substituting Eq. (3) into Eq. (2) yields the following:

$$\mathbf{\Phi}_{r\times R}\mathbf{\Psi}_{R\times R}\begin{bmatrix}\varepsilon_1\\ \varepsilon_2\\ \vdots\\ \varepsilon_R\end{bmatrix}_{R\times N}[\mathbf{Z}^T]_{N\times N}=\mathbf{\Phi}_{r\times R}\begin{bmatrix}\mathbf{V}_1\\ \mathbf{V}_2\\ \vdots\\ \mathbf{V}_R\end{bmatrix}_{R\times N} \tag{4}$$

Apply the transpose operation to both sides of the above equation results in:

$$\mathbf{Z}_{N\times N}\mathbf{I}^{CS}_{N\times r}=\mathbf{V}^{CS}_{N\times r} \tag{5}$$

where $\mathbf{V}^{CS}_{N\times r}$ represents the reconstructed excitation source, and $\mathbf{I}^{CS}_{N\times r}$ denotes the induced current generated by this source, expressed as:

$$[\mathbf{I}^{CS}]^T_{r\times N}=\mathbf{\Phi}_{r\times R}\mathbf{\Psi}_{R\times R}\begin{bmatrix}\varepsilon_1\\ \varepsilon_2\\ \vdots\\ \varepsilon_R\end{bmatrix}_{R\times N} \tag{6}$$

$$[\mathbf{v}^{CS}]^T_{r\times N}=\mathbf{\Phi}_{r\times R}\begin{bmatrix}\mathbf{V}_1\\ \mathbf{V}_2\\ \vdots\\ \mathbf{V}_R\end{bmatrix}_{R\times N} \tag{7}$$

In the monostatic scattering analysis, $\mathbf{I}^{CS}_{N\times r}$ can be expressed in terms of characteristic basis functions (CBFs) as follows:

$$\mathbf{I}^{CS}_{N\times r}=\mathbf{I}^{\text{CBFs}}_{N\times J}\boldsymbol{\alpha}_{J\times r} \tag{8}$$

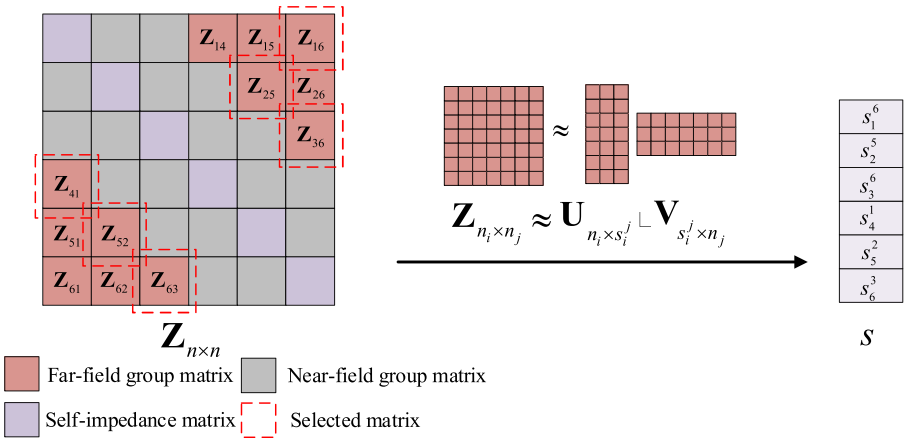

FIGURE 1. Schematic diagram of ACA row index.

where $\mathbf{I}^{\text{CBFs}}_{N\times J}$ represents the CBFs, and $\boldsymbol{\alpha}_{J\times r}$ denotes the coefficient vector. Substituting Eq. (8) into Eq. (5) yields:

$$\mathbf{Z}_{N\times N}\mathbf{I}^{\text{CBFs}}_{N\times J}\boldsymbol{\alpha}_{J\times r}=\mathbf{V}^{CS}_{N\times r} \tag{9}$$

A random selection of M rows from the impedance matrix $\mathbf{Z}_{N\times N}$ is performed to generate the restructured excitation source $\mathbf{V}^{CS}_{N\times r}$ through the following procedure:

$$\hat{\mathbf{Z}}_{M\times N}\mathbf{I}^{\text{CBFs}}_{N\times J}\boldsymbol{\alpha}_{J\times r}=\boldsymbol{\Theta}_1\boldsymbol{\alpha}_{J\times r}=\hat{\mathbf{V}}^{CS}_{M\times r} \tag{10}$$

where $\hat{\mathbf{Z}}_{M\times N}$ represents M rows randomly extracted from the impedance matrix $\mathbf{Z}_{N\times N}$, and $\hat{\mathbf{V}}^{CS}_{M\times r}$ represents M rows randomly extracted from the excitation matrix $\mathbf{V}^{CS}_{N\times r}$. $\boldsymbol{\Theta}_1$ is the sensing matrix $\hat{\mathbf{Z}}_{M\times N}\mathbf{I}^{\text{CBFs}}_{N\times J}$. Since $M<J$ results in an overdetermined system, the coefficient vector $\boldsymbol{\alpha}_{J\times r}$ is estimated via the least squares method, then substituted into Eq. (8) to compute $\mathbf{I}^{CS}_{N\times r}$, which is ultimately inserted into Eq. (6) to establish another CS theory framework.

$$[\mathbf{I}^{CS}]^T_{r\times N}=\boldsymbol{\Phi}_{r\times R}\boldsymbol{\Psi}_{R\times R}\begin{bmatrix}\varepsilon_1\\ \varepsilon_3\\ \vdots\\ \varepsilon_R\end{bmatrix}_{R\times N}=\boldsymbol{\Theta}_2\varepsilon_{R\times N} \tag{11}$$

Since the number of $r<R$, the set of equations at this level is smaller than the number of unknowns to be solved, and the recovery algorithm for the second step uses OMP. However, as it selects only a single atom in each iteration, multiple iterations are required. Moreover, due to the high column correlation of the measurement matrix caused by random row extraction, error accumulation is likely to occur [25].

2.2. The Proposed Method

In the aforementioned DCS method, the measurement matrix is constructed by randomly extracting rows, which is essentially an uncertain sampling method that does not consider the importance of individual row elements. To extract more meaningful rows from the impedance matrix, the new method employs the ACA to construct the measurement matrix.

The purpose of the ACA is to approximate $\mathbf{Z}$ by $\hat{\mathbf{Z}}$, as shown in the following formula:

$$\hat{\mathbf{Z}}=\mathbf{UV} \tag{12}$$

During this process, the ACA algorithm produces row indexes and column indexes, with the row indices essentially indicating the rows in the original matrix that contain critical information. Therefore, these generated row indices can be leveraged to construct the measurement matrix, instead of randomly selecting some rows from the original matrix. This method can effectively enhance the accuracy of the measurement matrix construction and improve the efficiency of the recovery process in monostatic electromagnetic scattering problems. The relevant process is shown in Fig. 1.

To ensure accuracy, the row indices with the max number of $s^6_1, s^5_2, s^6_3, ..., s^3_6$ are identified and converted into row-order numbers in the impedance matrix. Then, these row-order numbers are used as extraction guidelines when constructing the measurement matrix. So, the total number of rows extracted by ACA is $\sum s_i = s$, where s_i is the max number of s^j_i. Therefore, Eq. (9) can be transformed into:

$$\hat{\mathbf{Z}}_{s\times N}\mathbf{I}^{\text{CBFs}}_{N\times J}\boldsymbol{\alpha}_{J\times r}=\boldsymbol{\Theta}_1\boldsymbol{\alpha}_{J\times r}=\hat{\mathbf{V}}^{CS}_{s\times r} \tag{13}$$

where $\hat{\mathbf{Z}}_{s\times N}$ and $\hat{\mathbf{V}}^{CS}_{s\times r}$ represent s-row extracted from matrices $\mathbf{Z}_{N\times N}$ and $\mathbf{V}^{CS}_{N\times r}$, respectively. The CS recovery matrix $\boldsymbol{\Theta}_1=\hat{\mathbf{Z}}_{s\times N}\mathbf{I}^{\text{CBFs}}_{N\times J}$ calculates coefficients $\boldsymbol{\alpha}_{J\times r}$ using reconstruction algorithms. Since $s>J$, the system of equations becomes overdetermined, and therefore the coefficient $\boldsymbol{\alpha}_{J\times r}$ is obtained using the least squares method.

The aforementioned DCS in solving Eq. (11), where $\boldsymbol{\Theta}_2=\boldsymbol{\Phi}_{r\times R}\boldsymbol{\Psi}_{R\times R}$ is the recovery matrix, and $[\varepsilon_1\cdots\varepsilon_2\cdots\cdots\varepsilon_R]^T_{R\times N}$ is the required solution coefficient matrix. The recovery algorithm in the second step of this paper employs gOMP. Compared to OMP, which only selects the maximum value of the inner product, the multi-column selection mechanism of gOMP can more fully exploit the informational advantages offered by the measurement matrix constructed by ACA. After recovering the coefficient matrix $\varepsilon_{R\times N}$ using gOMP, the original induced current is obtained by

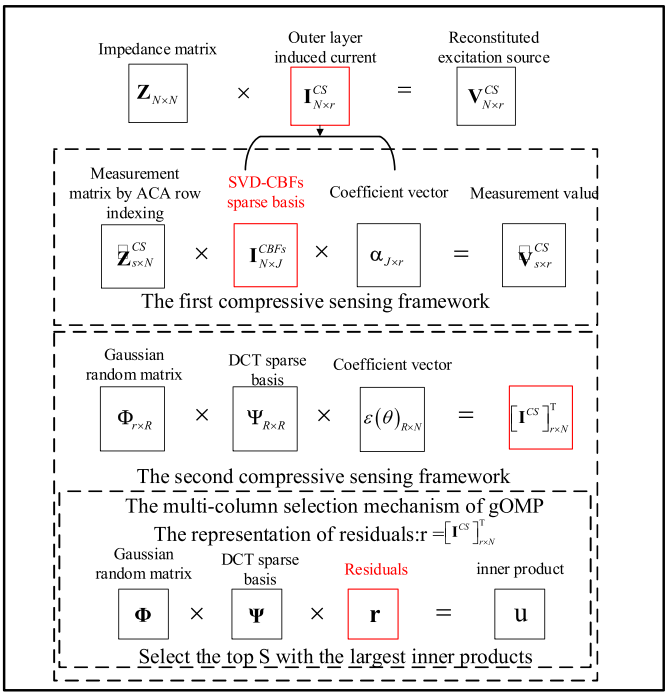

FIGURE 2. Flowchart of the proposed method.

substituting $\varepsilon_{R\times N}$ into Eq. (3). The flowchart illustrating the entire principle is shown in Fig. 2.

In Fig. 2, $\mathbf{r}$ is the residual, and u represents the inner product. The connection between them is as follows: the first layer constructs the measurement matrix through ACA, and the $\mathbf{I}^{CS}_{N\times r}$ is obtained through Eq. (11), which is then used as the excitation for the second layer. In the second layer, the gOMP algorithm initializes the $\mathbf{r}$ as $[\mathbf{I}^{CS}]^{T}_{r\times N}$, and in subsequent iterations, it remains related to $[\mathbf{I}^{CS}]^{T}_{r\times N}$. In the second-layer recovery phase, this paper employs the gOMP algorithm, which introduces a core enhancement by selecting S atoms ($S \geq 1$) exhibiting the strongest correlation with the residual error during each iteration. The mathematical formulation of this improvement can be expressed as follows:

$$S_t = \arg\max_{|\mathcal{J}|=s} \sum_{j\in\mathcal{J}} |\langle \mathbf{r}_{t-1}, \phi_j \rangle| \tag{14}$$

where $\mathbf{r}_{t-1}$ represents the residual from the $(t-1)$th iteration, and ϕ_j represents the jth column of the measurement matrix. In this process, the residual of the first layer $\mathbf{r}_1 = \left[\mathbf{I}^{CS}\right]^{T}_{r\times N}$ is transmitted to the second layer through implicit encoding, driving the optimization direction of the initial residual of the gOMP algorithm.

$$\mathbf{r}_t = y - A_t\hat{\theta}_t = y - A_t\left(A_t^T A\right)^{-1} A_t^r y \tag{15}$$

where y represents the $[\mathbf{I}^{CS}]^{T}_{r\times N}$, and A represents the $\mathbf{\Phi\Psi}$. Due to the low-correlation property of y, the statistical characteristics of the missing matrix A and y exhibit strong correlation, enabling the gOMP algorithm to quickly approximate the global optimal solution through multi-atom selection. The low column correlation of the measurement matrix constructed by ACA ensures that the S atoms selected in each iteration are approximately orthogonal, thereby avoiding information redundancy and accelerating the convergence of the support set. Additionally, the multi-atom selection mechanism enables the simultaneous capture of multiple key modes, mitigating the recovery bias caused by the accumulation of errors from single-atom selections. In summary, through the hierarchical optimization mechanism, the deterministic measurement matrix constructed by ACA is deeply coupled with the multi-atom selection strategy of gOMP to form an information-driven compression-recovery paradigm.

3. COMPLEXITY ANALYSIS

In the comparative analysis of measurement matrix construction methodologies, the measurement matrix has a dimension of $m \times n$, and the random extraction method extracts M rows, whereas ACA extracts s rows. Since ACA extracts rows containing key information, it achieves the same accuracy with fewer rows, hence $s < M$. The computational complexity for constructing the measurement matrix using random extraction is $O(Mn)$, whereas the computational complexity for constructing the measurement matrix using ACA row indexes is $O(sn)$. Therefore, for the same level of computational accuracy, the computational complexity of the measurement matrix is reduced. When signals in the second layer are recovered, the computational complexity of OMP and gOMP algorithms mainly consists of two parts: atom selection and least squares update. Assuming that the sparsity of the sensing matrix is K, the overall complexity of OMP can be decomposed as follows:

(1) Atom Selection: In each iteration, the inner product between the residual and each column of the measurement matrix needs to be computed, requiring $O(mn)$ operations. After K iterations, the total complexity of atom selection is $O(Kmn)$.

(2) Least Squares Update: In each iteration, a $t \times t$ least squares problem needs to be solved, where t is the current iteration count. In each iteration, the computation of $A^T A$ has a complexity of $O(mt^2)$, and solving the resulting linear system has a complexity of $O(t^3)$. Therefore, the overall complexity per iteration is generally considered to be $O(mt^2 + t^3)$. After K ($K = t$) iterations, the total complexity of the least squares update is $O(mK^3 + K^4)$.

Thus, the overall computational complexity of the OMP algorithm is $O(Kmn + mK^3 + K^4)$. For the gOMP algorithm, S atoms are selected per iteration, reducing the number of iterations to K/S. Similar to OMP, its complexity analysis is $O((Kmn + mK^3 + K^4)/S)$. Therefore, the overall computational complexity of the gOMP algorithm is reduced by approximately S times compared to OMP. In summary, comparing the complexity analysis of the two methods, it is evident that the new method has a lower complexity than the traditional method, significantly improving computational efficiency.

4. NUMERICAL RESULTS

To demonstrate the effectiveness of the proposed method, various 3D perfect electric conductor (PEC) targets are numerically simulated. The root-mean-square error (RMSE) of the monos-

TABLE 1. Correlation coefficients between measurement matrix and sparse basis.

Method	Random extraction	Uniform extraction	Proposed method
Correlation coefficient	$0.0074 + 0.1471\mathrm{i}$	$-0.0134 - 0.0146\mathrm{i}$	$0.0058 + 0.01254\mathrm{i}$

tatic radar scattering cross (RCS) of the targets is as follows:

$$\mathrm{RMSE} = \sqrt{\frac{1}{N_a}\sum_{i=1}^{N_a}\left(\boldsymbol{\sigma}_{\mathrm{cal}} - \boldsymbol{\sigma}_{\mathrm{MoM}}\right)^2} \tag{16}$$

where N_a represents the sample number, $\boldsymbol{\sigma}_{\mathrm{cal}}$ the calculation results of the proposed methods used, and $\boldsymbol{\sigma}_{\mathrm{MoM}}$ the calculation results of the MoM.

4.1. Perfect Electrical Conductor Cone

The first example is the monostatic scattering problem for a cube with a base radius of 1 m and a height of 2 m and vibrating at 400 MHz. The target is discretized into 6970 triangular elements, yielding 10455 unknowns. Then, the cone is divided into 15 blocks and extended in all directions according to $\Delta = 0.15\lambda$, resulting in 21946 unknowns, and 1665 CBFs were obtained.

First, Table 1 presents the correlation coefficients between the measurement matrix $\hat{Z}$ and sparse matrix $\boldsymbol{\Psi}$ constructed using the random extraction and uniform extraction strategies, as well as the proposed method. It is evident that the measurement matrix $\hat{\mathbf{Z}}$ constructed using the proposed method exhibits a weak correlation with the sparse transformation matrix $\boldsymbol{\Psi}$ satisfying the RIP [26], which ensures the accurate reconstruction of the sparse coefficient $\boldsymbol{\alpha}$.

Next, to verify the convergence of gOMP, Fig. 3 compares the impact of the number of selected atoms S on the RMSE, where angle represents the rows of the sensing matrix $\boldsymbol{\Theta}_2$. As shown in Fig. 3, the RMSE generally decreases with the increase of S, so the value of S is taken as $0.1 * \mathrm{angle}$.

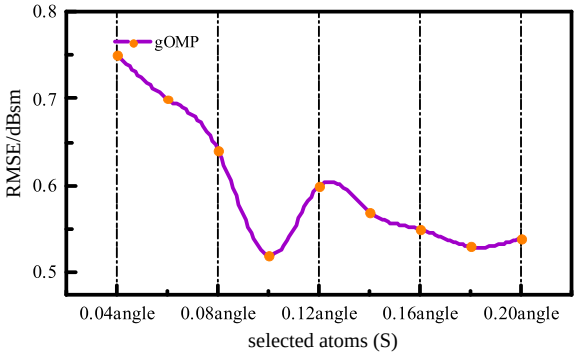

FIGURE 3. The RMSE for different selected atoms.

To demonstrate the benefits of the proposed method, Fig. 4 illustrates the time consumption and RMSE values of the traditional DCS with OMP (DCS-OMP) and DCS with gOMP (DCS-gOMP) under different extraction conditions. Fig. 5 shows the time consumption and RMSE values of the method incorporating ACA combined with OMP (DCS-ACA-OMP) and with gOMP (DCS-ACA-gOMP) under different thresholds of ACA.

The green point in Fig. 4(a) indicates that the total computing time is 4479.13 s; the RMSE is 0.96; and the number of rows extracted is 5277 when M/N are taken to be 0.5. The green dot in Fig. 4(b) indicates that when the RMSE is 0.64, the total computation time is 1891.73 s, and the number of rows extracted is 5277, when M/N are taken to be 0.5, where N is the number of unknowns, and M is the number of randomly selected rows. Moving on to Fig. 5(a), the green point represents 4424.26 s of total time and 3052 rows extracted with an RMSE of 0.94. Similarly, the green point of Fig. 5(b) indicates that with 3150 rows extracted, the total time is 1844.09 s, and the RMSE is 0.52. From this, by comparing Fig. 4(b) and Fig. 5(b), we can see the advantage of ACA. By examining all four figures in Fig. 4 and Fig. 5, it is evident that the recovery effect of gOMP is indeed better than that of OMP, but the combination of ACA and gOMP clearly yields significantly better results than just changing the algorithm alone, further illustrating that the gOMP algorithm is better at leveraging the information optimization brought by ACA.

As shown in Fig. 5, as the ACA threshold increases, the number of selected row indices decreases, which speeds up the solution process but reduces accuracy. Conversely, lowering the threshold causes ACA to select more rows, which reduces the RMSE but increases the computational time. To balance time and RMSE, and based on the content displayed in the four graphs, the random sampling ratio M/N for DCS is set to 0.5 so that 5277 rows are extracted. At the same time, the threshold for ACA in DCS-ACA is set to 5E-7 during the measurement matrix construction. This resulted in the extraction of 3150 rows, which took 1844.09 s and had an RMSE of 0.52. Fig. 6 then compares the RCS obtained using the proposed method and the conventional method. As can be observed from the figure, the numerical results obtained using the proposed method are in good agreement with the MoM results.

4.2. Perfect Electrical Conductor Cylinder

In the second example, monostatic scattering at 900 MHz is analyzed for a cylindrical object with a 0.5-meter radius and 1-meter height. The object was initially meshed into 16,142 triangular elements, resulting in 24,213 unknowns. It was then segmented into 12 subdomains, each of which was uniformly extended in all directions based on $\Delta = 0.15\lambda$, resulting in 42264 unknowns, and 2395 CBFs were obtained. Set the random extraction ratio of DCS to 0.5 so that 12106 rows are extracted, and the threshold for ACA in DCS-ACA is set to 1E-8. This resulted in the extraction of 6360 rows. Meanwhile, Fig. 7 shows the RCS results for a cylinder. Obviously, the calculated

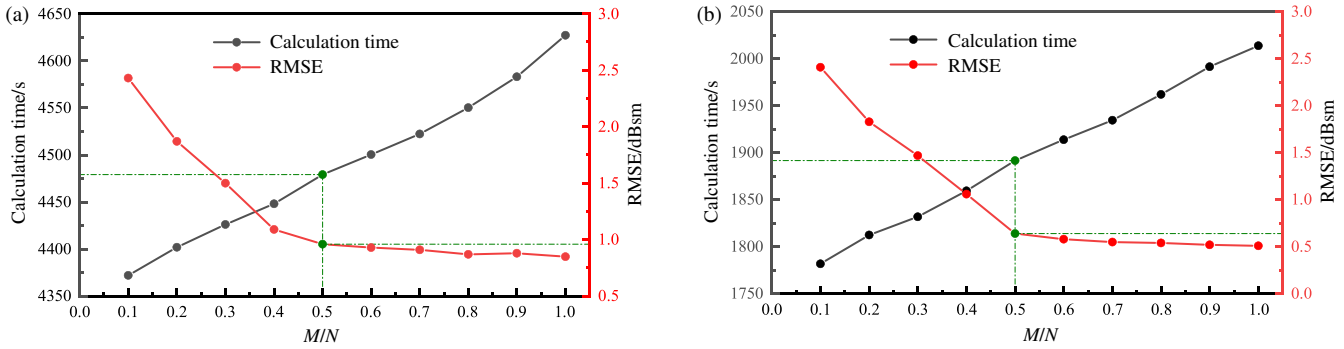

FIGURE 4. The time and RMSE for different extraction steps for DCS. (a) The time and RMSE of different extraction steps for DCS-OMP. (b) The time and RMSE of different extraction steps for DCS-gOMP.

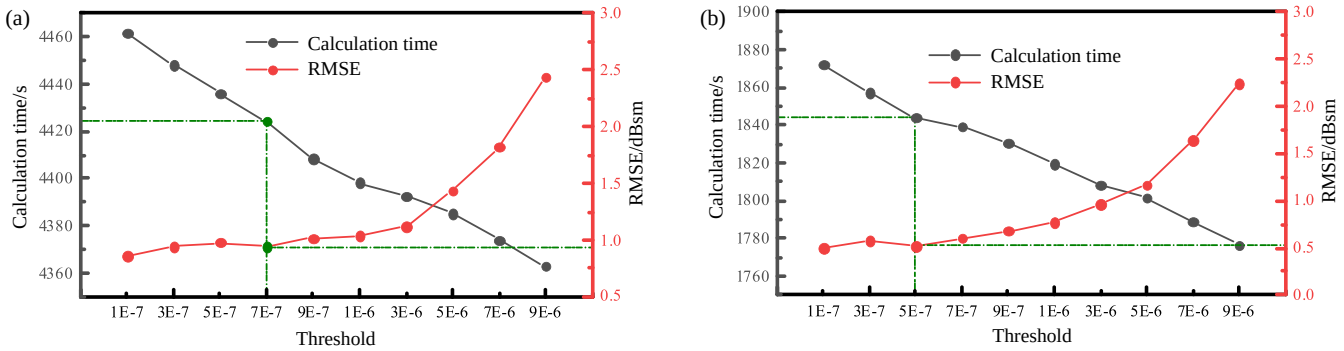

FIGURE 5. The time and RMSE for different extraction steps for DCS-ACA. (a) The time and RMSE of different extraction steps for DCS-ACA-OMP. (b) The time and RMSE of different extraction steps for DCS-ACA-gOMP.

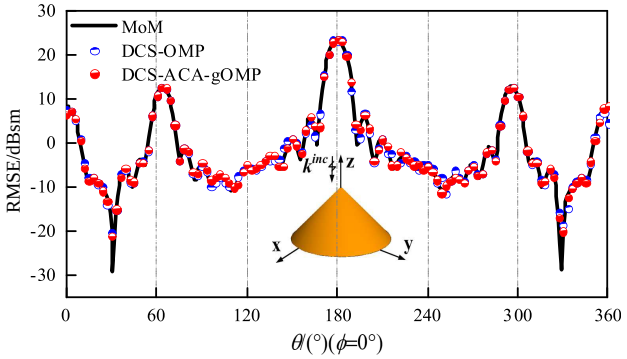

FIGURE 6. Monostatic RCS of the cone in horizontal polarization.

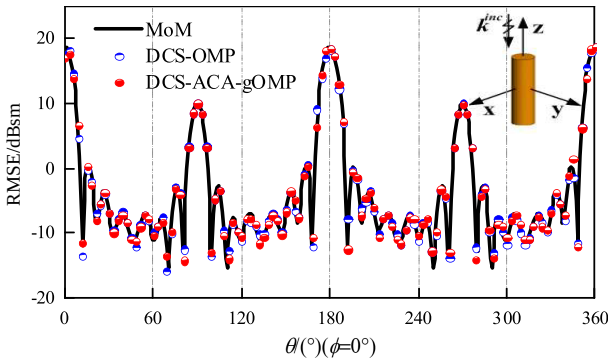

FIGURE 7. Monostatic RCS of the cylinder in horizontal polarization.

result of the proposed method is in excellent agreement with the MoM.

4.3. Perfect Electrical Conductor Missile

The last example considers the monostatic RCS of a missile at 4.8 GHz. The target is discretized into 52782 triangular surface elements, generating a total of 79173 unknowns. Moreover, the target is divided into 26 blocks and expanded in each direction according to $\Delta = 0.15\lambda$ on each block; therefore, 114902 unknowns are obtained, and 6835 CBFs were obtained. Fig. 8 depicts the monostatic RCS results for missile in vertical polarization, calculated using MoM, DCS, and the proposed method. The figure demonstrates that the RCS results calculated by the DCS-ACA and the MoM exhibit strong agreement.

Table 2 shows the computation time and RMSE for three different 3D targets using the two methods. It should be noted that the impedance matrix in the proposed method is partially filled. In the two methods, "Solving time" refers to the time consumed by the first least squares solution and the second-step recovery process using OMP or gOMP. As can be seen from Table 2, DCS-ACA not only enhances accuracy but also saves more time cost than DCS. Numerical simulation results demonstrate that under identical extracting conditions, the proposed method exhibits significant advantages over conventional techniques, achieving respective improvements of 45%, 37%, and 44% in

TABLE 2. Simulation time of different processes.

Model	Number of unknowns	Method	Extracted rows	Row index time (s)	Sensing matrix time (s)	Current solving time (s)	Total time (s)	RMSE (dBsm)
Cone	10455	DCS-OMP	5227	-	45.17	84.06+3633.72	4479.13	0.96
		DCS-ACA-gOMP	3150	14.83	41.96	52.12+1844.09	1844.09	0.52
Cylinder	24213	DCS-OMP	12106	-	296.41	358.63+8825.52	12363.8	0.9
		DCS-ACA-gOMP	6360	111.93	260.71	209.57+2418.47	5735.63	0.56
Missile	79173	DCS-OMP	39586	-	9820.86	3449.11+69404.2	116790	2.05
		DCS-ACA-gOMP	19418	4091.3	8442.93	1933.71+54138.6	54138.6	1.13

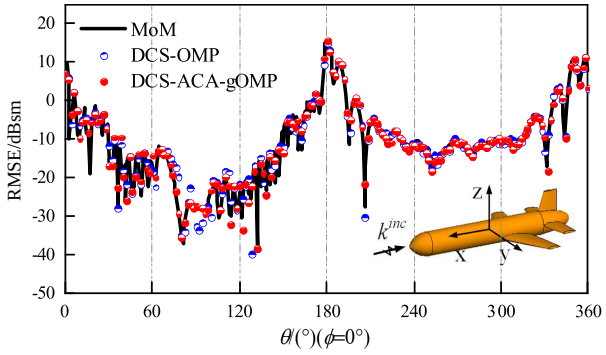

FIGURE 8. Monostatic RCS of the missile in horizontal polarization.

reconstruction accuracy, along with computational time reductions of 58%, 54%, and 53%. Although a significant portion of the improvement stems from the gOMP algorithm, the advantages of ACA row indexing are still evident. Moreover, it is clear that combining with gOMP brings further improvements compared to combining with OMP.

However, our code is not implemented in an efficient manner compared to commercial solvers like FEKO. This is because FEKO has undergone extensive optimization, and therefore, a direct comparison of computational times is not very meaningful. Our method is primarily intended to lay the groundwork for future research and optimization.

5. CONCLUSION

Aiming at the issues of low efficiency and accuracy in traditional DCS, this paper proposes a novel DCS technique. First, the random sampling in the first compression layer is replaced by ACA row index extraction to construct the measurement matrix. In addressing monostatic scattering problems, the integration of the gOMP algorithm with ACA demonstrates a synergistic enhancement in computational performance. The ACA preprocessing stage efficiently identifies highly correlated atomic indices, which are then leveraged by gOMP through its multi-column residual selection mechanism. This combined approach ensures approximate orthogonality among selected atoms, thereby mitigating error propagation and accelerating the convergence of the support set. Numerical simulations validate the effectiveness of the novel DCS framework in addressing electromagnetic scattering problems.

ACKNOWLEDGEMENT

This work was supported in part by the National Natural Science Foundation of China under Grant No. 62071004 and No. 61401003, and in part by the Graduate Innovation Fund of Anhui University of Science and Technology under grant No. 2025cx2070.

REFERENCES

[1] Song, J., C.-C. Lu, and W. C. Chew, "Multilevel fast multipole algorithm for electromagnetic scattering by large complex objects," *IEEE Transactions on Antennas and Propagation*, Vol. 45, No. 10, 1488–1493, 1997.

[2] Prakash, V. V. S. and R. Mittra, "Characteristic basis function method: A new technique for efficient solution of method of moments matrix equations," *Microwave and Optical Technology Letters*, Vol. 36, No. 2, 95–100, 2003.

[3] Sun, Y. F., Y. Zhang, S. J. Xu, and X. Q. Chen, "EM scattering analysis of 2-D multiple conducting cylinders using characteristic basis function method," *Chinese Journal of Radio Science*, Vol. 21, No. 2, 229–232, 2006.

[4] Xu, Y., H. Yang, J. Lu, W. Yu, W. Yin, and D. Peng, "Improved synthetic basis functions method for nonperiodic scaling structures with arbitrary spatial attitudes," *IEEE Transactions on Antennas and Propagation*, Vol. 65, No. 9, 4728–4741, 2017.

[5] Donoho, D. L., "Compressed sensing," *IEEE Transactions on Information Theory*, Vol. 52, No. 4, 1289–1306, 2006.

[6] Liu, J., X.-L. Huang, and P. Wang, "Compressive spectrum sensing with temporal-correlated prior knowledge mining," *Wireless Communications and Mobile Computing*, Vol. 2021, No. 1, 5539697, 2021.

[7] Wang, R., J.-B. Guo, J.-P. Hui, Z. Wang, H.-J. Liu, Y.-N. Xu, and Y.-F. Liu, "Statistical compressive sensing based on convolutional Gaussian mixture model," *ACTA Physica Sinica*, Vol. 68, No. 18, 180 701–180 712, 2019.

[8] Zhong, Y., J. Zhang, X. Cheng, G. Huang, Z. Zhou, and Z. Huang, "Reconstruction for block-based compressive sensing of image with reweighted double sparse constraint," *EURASIP Journal on Image and Video Processing*, Vol. 2019, No. 1, 1–14, 2019.

[9] Chen, M. S., F. L. Liu, H. M. Du, and X. L. Wu, "Compressive sensing for fast analysis of wide-angle monostatic scattering problems," *IEEE Antennas and Wireless Propagation Letters*, Vol. 10, 1243–1246, 2011.

[10] Chai, S.-R. and L.-X. Guo, "A new method based on compressive sensing for monostatic scattering analysis," *Microwave and Optical Technology Letters*, Vol. 57, No. 10, 2457–2461, 2015.

[11] Kong, M., M. Chen, X. Cao, L. Zhang, Q. Qi, and X. Wu, "Fast analysis of local current distribution for electromagnetic scattering problems of electrically large objects," *IEEE Access*, Vol. 8, 127 640–127 647, 2020.

[12] Chai, S.-R. and L.-X. Guo, "Integration of CS into MoM for efficiently solving of bistatic scattering problems," *IEEE Antennas and Wireless Propagation Letters*, Vol. 15, 1771–1774, 2016.

[13] Kong, M., M. S. Chen, B. Wu, and X. L. Wu, "Fast and stabilized algorithm for analyzing electromagnetic scattering problems of bodies of revolution by compressive sensing," *IEEE Antennas and Wireless Propagation Letters*, Vol. 16, 198–201, 2016.

[14] Cao, X., M. Chen, Q. Qi, M. Kong, J. Hu, L. Zhang, and X. Wu, "Solving electromagnetic scattering problems by underdetermined equations and Krylov subspace," *IEEE Microwave and Wireless Components Letters*, Vol. 30, No. 6, 541–544, 2020.

[15] Wang, Z., H. Yuan, Y. Sun, W. Nie, and P. Wang, "Block-based Krylov subspace basis functions for solving bistatic scattering problems," *IEEE Antennas and Wireless Propagation Letters*, Vol. 22, No. 10, 2561–2565, 2023.

[16] Wang, Z., P. Wang, Y. Sun, and W. Nie, "Fast analysis of bistatic scattering problems for three-dimensional objects using compressive sensing and characteristic modes," *IEEE Antennas and Wireless Propagation Letters*, Vol. 21, No. 9, 1817–1821, 2022.

[17] Gao, Y., M. F. Akbar, and G. N. Jawad, "Stabilized and fast method for compressive-sensing-based method of moments," *IEEE Antennas and Wireless Propagation Letters*, Vol. 22, No. 12, 2915–2919, 2023.

[18] Wang, Z.-G., W.-Y. Nie, and H. Lin, "Characteristic basis functions enhanced compressive sensing for solving the bistatic scattering problems of three-dimensional targets," *Microwave and Optical Technology Letters*, Vol. 62, No. 10, 3132–3138, 2020.

[19] Dong, D., Z. Wang, W. Nie, F. Guo, Y. Sun, P. Wan, and C. Li, "Adaptive cross approximation accelerates compressive sensing-based method of moments for solving electromagnetic scattering problems," *Progress In Electromagnetics Research C*, Vol. 146, 45–53, 2024.

[20] Kong, M., M. S. Chen, X. Y. Cao, J. B. Zhu, X. J. Kuang, Q. Qi, and X. L. Wu, "Fast electromagnetic scattering analysis of inhomogeneous dielectric objects over a wide incident angle," *IEEE Antennas and Wireless Propagation Letters*, Vol. 20, No. 8, 1527–1531, 2021.

[21] Cao, X., M. Chen, X. Wu, M. Kong, J. Hu, and Y. Zhu, "Dual compressed sensing method for solving electromagnetic scattering problems by method of moments," *IEEE Antennas and Wireless Propagation Letters*, Vol. 17, No. 2, 267–270, 2018.

[22] Ma, Y., Z. Wang, W. Nie, Y. Sun, J. Wu, and P. Wang, "Novel dual compressive sensing method for solving the monostatic scattering problems of three-dimensional target," *Electromagnetics*, Vol. 43, No. 8, 577–590, 2023.

[23] Gao, Y., M. F. Akbar, G. N. Jawad, and L. Cui, "Dual-layer compressive sensing scheme incorporating adaptive cross approximation algorithm for solving monostatic electromagnetic scattering problems," *IEEE Access*, Vol. 12, 97 572–97 580, 2024.

[24] Zhang, Y.-W., V. Sorkin, Z. H. Aitken, A. Politano, J. Behler, *et al.*, "Roadmap for the development of machine learning-based interatomic potentials," *Modelling and Simulation in Materials Science and Engineering*, Vol. 33, No. 2, 023301, 2025.

[25] Ding, J., L. Chen, and Y. Gu, "Perturbation analysis of orthogonal matching pursuit," *IEEE Transactions on Signal Processing*, Vol. 61, No. 2, 398–410, 2013.

[26] Tropp, J. A. and A. C. Gilbert, "Signal recovery from random measurements via orthogonal matching pursuit," *IEEE Transactions on Information Theory*, Vol. 53, No. 12, 4655–4666, 2007.